

Gravity-aware Grasp Generation with Implicit Grasp Mode Selection for Underactuated Hands

Tianyi Ko^{*†}, Takuya Ikeda^{*}, Thomas Stewart^{*}, Robert Lee^{*}, Koichi Nishiwaki^{*}

Abstract—Learning-based grasp detectors typically assume a precision grasp, where each finger only has one contact point, and estimate the grasp probability. In this work, we propose a data generation and learning pipeline that can leverage power grasping, which has more contact points with an enveloping configuration and is robust against both positioning error and force disturbance. To train a grasp detector to prioritize power grasping while still keeping precision grasping as the secondary choice, we propose to train the network against the magnitude of disturbance in the gravity direction a grasp can resist (gravity-rejection score) rather than the binary classification of success. We also provide an efficient data generation pipeline for a dataset with gravity-rejection score annotation. In addition to thorough ablation studies, quantitative evaluation in both simulation and real-robot clarifies the significant improvement in our approach, especially when the objects are heavy.

I. INTRODUCTION

Power grasp [1] is a grasping mode where the fingers and palm contact the object at multiple points. Since the object is enveloped by the fingers, the grasp is robust against both initial position error and post-grasp force disturbance. Current state-of-the-art machine-learning-based grasp detectors [2]–[9], though, only assume precision grasp [1] where each finger has only one contact point. Even though precision grasping is easier to handle in both the data generation and learning aspects, its limited contact region makes the grasp fragile. A typical failure mode of a precision grasp by a parallel-jaw gripper is that the object rotates around the axis connecting the two contact points, during which translational displacement also occurs to result in dropping the object. The small contact region also imposes a high demand for accurate hand-eye calibration and hand positioning, which is challenging for low-cost manipulators or those under low-impedance control for safety. To this end, in this paper, we introduce a data generation and learning framework to learn power grasping in addition to the common precision grasping. Figure 2 (a) illustrates a typical precision grasp and power grasp.

Underactuated hands [10] have a larger number of joints than the number of actuation. This passive compliance allows the hand to adapt to various objects with non-typical geometries without explicitly controlling each joint. Since it makes power grasping easier, this work focuses on utilizing underactuated hands, or more specifically, Robotiq 2F-85 [11]. However, such mechanically automatic property makes learning power grasps challenging because whether the grasp



Fig. 1. While existing works only handle precision grasping, power grasping is more robust against both initial position error and post-grasp force disturbance. We propose a data generation pipeline and neural network model that prioritizes power grasping if applicable (left) but implicitly switches back to precision grasping if power grasping is not available due to collision with the table (middle) or other objects (right.)

is a power grasp or a precision grasp cannot be explicitly controlled but only decided through the interaction between the object and the hand’s link mechanism. In addition, since a power grasp requires the fingers to wrap around the object, it is not always possible due to collisions with the environment, such as the tabletop or other objects (see Fig. 1 middle and right.) To this end, we propose a neural network architecture that prioritizes power grasping if applicable but implicitly switches back to precision grasping if power grasping is not available. More specifically, while prior works [2]–[9] only estimate the success probability of a grasp, we handle two values, namely (i) *gravity-rejection score* that represents the magnitude of disturbance in the gravity direction a grasp can support, which implicitly encourages power grasping since our data generation pipeline labels higher score for power grasps, and (ii) *grasp validness* which implicitly rejects grasps where the fingers will collide with the environment or it is too big for the hand to grasp.

Our contributions are as follows:

- A grasp data generation pipeline for a dense annotation of grasp poses and the magnitude of disturbance in the gravity direction a grasp can support (*gravity-rejection score*) for both power grasping and precision grasping of underactuated hands.
- A neural network model that prioritizes power grasping if applicable but implicitly switches back to precision grasping if power grasping is not available, by learning both *gravity-rejection score* and *grasp validness*.
- A novel visualization approach to intuitively understand the network output. A thorough simulation evaluation

^{*} T. Ko, T. Ikeda, T. Stewart, R. Lee, K. Nishiwaki are with Woven by Toyota, Inc., 3-2-1 Nihonbashi-Muromachi, Chuo-ku, Tokyo, Japan.

[†] Corresponding author. tianyi.ko@woven.toyota

and ablation study based on a novel evaluation procedure in which the grasp is performed against various object weights. A real-system quantitative evaluation that shows the significant improvement of our approach.

II. RELATED WORKS

A. Training Data for Learned Grasp Detectors

The quality of the training data plays a critical role in any machine-learning-based system. For grasp detectors, it is common to take the synthetic approach since gathering real physics data is costly. Mahler et al. [12] labeled grasps with a score based on the robust grasp wrench space analysis [13]. Fang et al. [14] and Wang et al. [7] adopted the same metrics as [12]. Fang et al. [15] further extended [7] by adding a score based on the distance from the object’s center of mass. Qin et al. [2] first sampled grasps for each object and then projected them to cluttered scenes to reduce the computational cost, with antipodal score as the metric. Zhao et al. [3] took the same approach as [2]. Cai et al. [9] also took the two-staged approach but employed Q1 metric [16] in addition to the antipodal score. In this paper, we also adopt the two-staged approach, but it differs from other works in the grasp generation of power grasps of an underactuated hand and evaluation metrics for the *gravity-rejection score*.

While analytical metrics are computationally efficient, it is difficult to capture all aspects of a contact, such as contact force distribution or motion after a slip. Kappler et al. [17] reported that a simulation-based approach achieves a better performance. Zhou et al. [18] and Eppner et al. [19] followed [17] in shaking the hand in a gravity-less simulation. Breyer et al. [5] evaluated grasps by actually lifting the object in a simulation and classified its success or failure. Jiang et al. [6] also followed [5]. Huang et al. [8] further shake the hand after lifting the object to select only robust grasps. Those prior works use the simulator to get a set of valid grasps. However, such binary classification suffers from the sim-to-real gap since the absolute value of success or failure highly depends on the simulator’s contact model and parameters. In this paper, we also take a simulation-based approach, but we acquire a continuous spectrum of the *gravity-rejection score* to train the neural network to prioritize grasps with higher safety margins, such as power grasps. In addition, we propose an approximation to allow the two-staged approach to relax the high computation cost of the simulation-based approaches. Section III details our data generation pipeline.

B. Grasp Representation in Learned Grasp Detectors

There are two major approaches to representing grasp with neural networks: sample-and-evaluate approach [3], [7], [12], [20]–[22] and feed-forward approach [2], [4]–[6], [8], [9], [23]. In the first approach, the network is only responsible for classifying and scoring the point cloud that is cropped and transformed to the hand coordinate; thus, it is extendable for power grasps. The multimodality that both power grasping and precision grasping may exist, though, prohibits using sample-efficient techniques such as sampling Darboux frame from the object surface [20], [22]. In order to avoid power

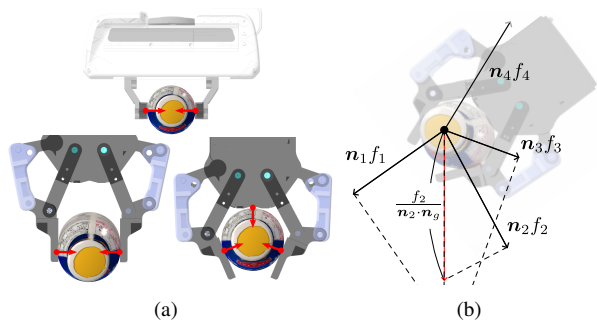


Fig. 2. (a) Most works assume a precision grasp (top, bottom left) due to its simplicity. A power grasp (bottom right) allows a more robust grasp thanks to the larger number of contacts. (b) Illustration of Eq. 1 which approximate the multidimensional *disturbance-rejection score* to the gravity direction *gravity-rejection score*.

grasping to induce a large computation time in the sampling stage due to the larger search space than other works, we opt for the feed-forward approach.

A large number of works in 3D grasp detection [2]–[4], [7]–[9], [21], [22], take point cloud as the input. Extending the combination of point cloud representation and feed-forward network to power grasps, though, is challenging. Qin et al. [2] regressed translation offset and rotation of the hand from each point on the object surface. Cai et al. [9] used the location and normal of the points on the object surface to decide five degrees of freedom of the hand and regressed the remaining in-plane rotation. Since [2], [9] interpreted the surface point as candidates that face the hand, a set of precision grasp and power grasp poses may be assigned to a single point, leading to representation ambiguity. Sundermeyer et al. [4] and Huang et al. [8], on the other hand, interpreted the surface points as candidates of contact and reported a superior performance. Contact points of a power grasp, however, significantly differ among the object size, making explicit contact representation challenging (see Fig. 2 (a).)

Morrison et al. [23] employed a 2D fully convolutional network to infer per-pixel grasp probability and hand yaw angle from a depth image. Breyer et al. [5] extended it to 3D grasp detection with TSDF (truncated signed distance function) as the input, where a 3D fully convolutional network estimated per-voxel grasp probability and rotation in $SO(3)$. Jiang et al. [6] followed [5] and jointly learned an implicit representation. The fully convolutional architecture is suitable to be extended for power grasps since (i) a precision grasp and a power grasp are assigned to different voxels (see Fig. 2 (a) bottom, the distance from the object differs for the two grasp modes), (ii) a precision grasp and a power grasp that grasps similar location on the object tends to have a similar rotation, thus we can expect a continuous grasp rotation field. In this work, we use the same backbone as [5], but differ in that the network is trained against both the continuous *gravity-rejection score* and the binary classification. Section IV details our network implementation.

III. SYNTHETIC DATA GENERATION WITH GRAVITY-REJECTION SCORE

Given a set of scenes (in this work, 5K) with multiple objects (in this work, 1-5) placed in a cluttered way (see Fig. 3 bottom), our target is to generate a dense annotation (in this work, 1.2K on average for each scene) of grasps with both power grasp and precision grasp mode, and label the *gravity-rejection score*, which stands for the magnitude of disturbance in the gravity direction the grasp can support. Following the previous works [2], [3], [9], we first generate per-object grasp poses. Unlike the case of precision grasp, where grasp poses can be generated by sampling antipodal points on the object’s surface, it is not trivial to generate power grasps by a purely geometric approach. In addition, for underactuated hands, the final contact state is decided through the interaction between the object and the finger mechanism. We, therefore, take a simulation-based approach where we perturb a precision grasp and simulate the contact process by closing the hand against the object in a simulator. Through the contact, the object settles in the hand, and we record the hand’s pose relative to the object.

In order to train a network to prioritize power grasp, we need a grasp metric that takes a higher value for power grasp. While analytical metrics [16] are computationally efficient, they assume each contact is independent. For underactuated hands, though, the contacts are tightly coupled through the parallel link mechanism. Following [5], [6], [8], we also take a simulation approach for the grasp evaluation. Our approach, though, differs from theirs in two aspects: (i) instead of performing the simulation at the scene level, we perform at the object level and project the *disturbance-rejection score* to the gravity direction of the scenes, which drastically reduces the computation cost; (ii) instead of evaluating a grasp by a success/fail binary label, we treat them as a continuous value.

At the object level, for each grasp, we apply an increasing external force on the object until it leaves the hand, and record the magnitude of the force as *disturbance-rejection score*. By applying the force on the object’s center of mass, we can encourage the network to prioritize grasping near the center of mass, in addition to prioritizing power grasping. As the gravity direction is unknown at this stage, we perform this evaluation in multiple directions, resulting in a n -dimensional score where n is the number of the directions. In this work, we selected $n = 6$. Considering that we employed 75 objects and generated 3K grasps per object on average, we can reduce the number of simulations to 1/24 of the cases where each grasp is evaluated at the scene level by the simulation.

In order to project the n -dimensional *disturbance-rejection score* to the scene’s gravity direction to acquire the one-dimensional *gravity-rejection score* f_g , we take the following approximation:

$$f_g = \min_{\{i | \mathbf{n}_i \cdot \mathbf{n}_g > \epsilon\}} \frac{f_i}{\mathbf{n}_i \cdot \mathbf{n}_g} \quad (1)$$

where $\mathbf{n}_g \in \mathbb{R}^3$ is the unit vector heading the direction of gravity, f_i is the i -th element of the *disturbance-rejection*

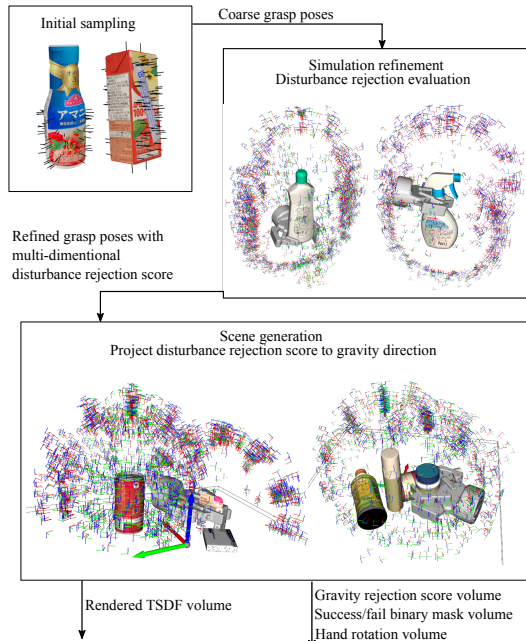


Fig. 3. Schematic of our data generation pipeline. We sample precision grasps based on the antipodal score and coarse power grasps by heuristically shifting the precision grasps (top-left). Those initial grasps are refined through grasp simulation (top-right). We apply external force in multiple directions and acquire a multi-dimensional *disturbance-rejection score* for each grasp. Finally, we create multi-object scenes and project per-object grasp poses to the scene to acquire the training data (bottom). The *disturbance-rejection score* is projected to the scene’s gravity direction to acquire the *gravity-rejection score*.

score, $\mathbf{n}_i \in \mathbb{R}^3$ is the unit vector heading the direction of the i -th disturbance, and ϵ is a small positive value. Figure 2 (b) illustrates the approximation and Fig. 3 illustrates the whole data generation pipeline.

IV. NETWORK ARCHITECTURE AND TRAINING

Given a single depth image as the input, our target is to infer a set of grasp poses in SE(3) with *gravity-rejection score*. At the inference time, the robot tries to execute the first reachable and collision-free grasp with the highest *gravity-rejection score*. This differs from other works that estimate the probability of the grasp: a higher *probability* means the network is more *confident*, but it doesn’t mean the grasp is more *robust*; in our case the *gravity-rejection score* has a unit of [N], which directly represents the grasp’s robustness in the gravity direction.

As discussed in Section II-B, we take a 3D fully convolutional network as the backbone following [5], but with a *gravity-rejection score* regression head. Unlike the case of [5], where both positive and negative samples were included in the dataset, our data generation pipeline described in Sec. III only provides positive samples. We therefore train the *gravity-rejection score* head with L2 loss against positive examples only, leaving the invalid grasp regions as out-of-domain. While [5] introduced a heuristic filter to remove out-of-domain voxels, in this work, we propose to learn a *grasp validness* head to classify whether the voxel is

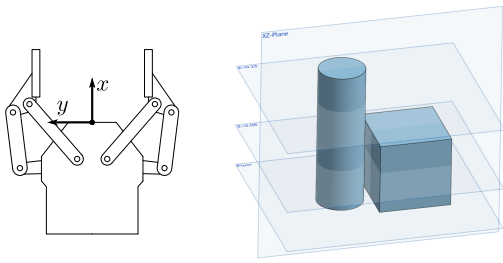


Fig. 4. TCP coordinate definition (left) and scene for the static network input/output analysis (right.) A $\varnothing 65 \times 200$ mm cylinder and a $100 \times 80 \times 100$ mm cube are placed on the surface and the input/output of the network is visualized with the three blue-colored cross-sections.

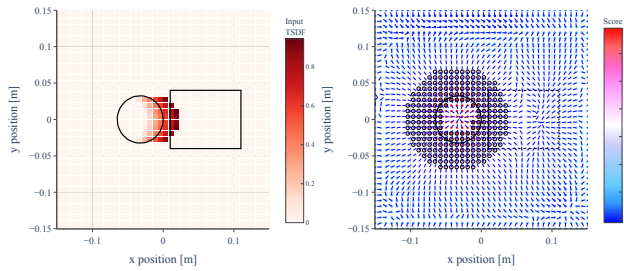


Fig. 5. Input TSDF volume (left) and output grasp volume (right) with $z = 0.15$ cross-section. The markers with black-circle are voxels with positive classification. The short blue lines are the hand approach direction.

out-of-domain. The evaluation in Sec. V-A shows that this classification head is also effective in collision avoidance or rejecting grasping an improper region. As the training data is densely annotated, we fill all voxels without a grasp label as *invalid* and use a weighted cross-entropy loss for the training.

V. EXPERIMENT AND EVALUATION

A. Analysis of Gravity-Rejection Score and Classification

This subsection provides a qualitative analysis of the network output *gravity-rejection score* and *grasp validity*. We placed two primitive objects in the simulator: a $\varnothing 65 \times 200$ mm cylinder at $[-0.0325, 0, 0]$ m location and a $100 \times 80 \times 100$ mm cube at $[0.06, 0, 0]$ m location. Even though these two objects were not included in our dataset, their geometries fall into our typical cases, such as water bottles and daily goods boxes, because we target home-use products. We placed a single camera at $[0.5, 0, 0.5]$ [m] and plotted the input TSDF volume and output grasp volume. Figure 4 left illustrates the TCP (tool center point) coordinate, and Fig. 4 right shows the experiment scene. We plot the cross-sections by $z = 0.15$, $z = 0.08$ and $y = 0$ plane in Fig. 5, 6, 7 respectively.

The color bar on the right plot of the figures stands for the *gravity-rejection score*, which is a continuous field that takes a higher value when it's closer to the object. This distribution encourages power grasping, as shown in Fig. 2 (a). Since the *gravity-rejection score* head is only trained against valid grasps, its output for the out-of-domain voxels is incorrect, e.g., it takes an even higher value inside the object or still takes a medium score at too-far-from-the-object region. The

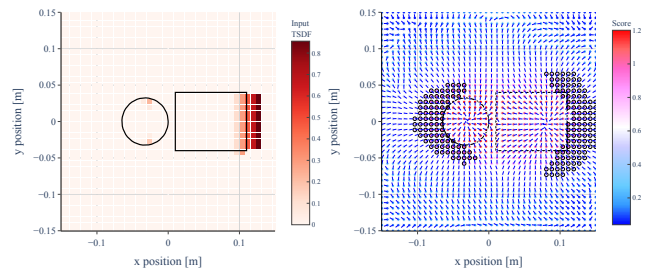


Fig. 6. Input TSDF volume (left) and output grasp volume (right) with $z = 0.08$ cross-section. The score prioritizes power grasps while the classification rejects grasps with collision or with too-big width.

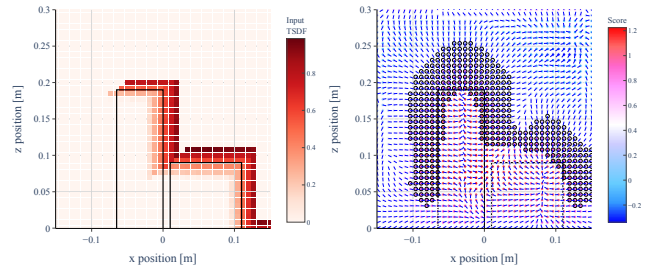


Fig. 7. Input TSDF volume (left) and output grasp volume (right) with $y = 0$ cross-section. Even for the region invisible to the camera, the network well predicts grasp poses. The classification properly removes grasps where the palm may collide with other objects.

markers surrounded by a black circle represent the voxel with a higher *grasp validity* than the threshold. The three figures show that this classification is highly effective in rejecting those too-close or too-far grasps. In addition, in Fig. 6, grasps at $x = 0$, $y = \pm 0.05$ region are rejected. Indeed, grasping this region is impossible due to the limitation of the hand's maximum openness of 85 mm; thus, training data does not contain such grasps. Similarly, in Fig. 7 grasps at $x = 0.03$, $y = 0.12$ are rejected. This is also reasonable since the hand's palm will collide with the objects to grasp this concave part.

B. Simulation Benchmark

In this subsection, we compare our approach (*ours*) with two baselines: Breyer et al. [5] (*VGN*) since we share the same backbone, and Huang et al. [8] (*VN-EdgeGraspNet*) since they reported state-of-the-art performance. While both [5] and [8] provide a pre-trained weight for Franka Emika's hand [24]¹, we target Robotiq 2F-85 [11] hand; thus, we created a simulation model for both hands with an identical grasp force and contact parameters². As the simulator, we used Drake [25] since its hydroelastic contact model [26] allows a stable simulation of power grasping by hands with a passive parallel-link mechanism. To clarify the effect of power grasps, we also trained our model (*Ours-Precision*) for Franka Emika's hand with only precision grasp annotation in the training data.

¹ [8] performed a real-robot validation with the Robotiq gripper in their paper, but they only made Franka Emika version's weight public.

²We set 40 N for grasp force, 0.75/0.5 for static/dynamic friction coefficient, 5 for Hunt Crossley dissipation, 10^8 for hydroelastic-modulus.

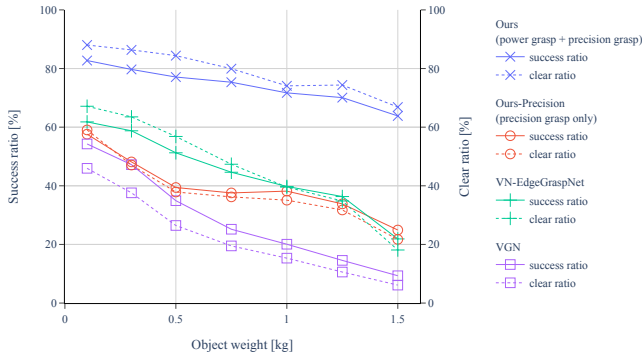


Fig. 8. Success ratio (SR) and clear ratio (CR) against multiple object weights. Our approach significantly outperformed the baselines, especially when the objects were heavy, showing the advantage of power grasp.

For the quantitative evaluation, we used the same metrics as [2], [3], [5], [6], [8], [9]: success ratio (SR) representing the number of successful grasps divided by the number of total trials, and clear ratio (CR) representing the number of successful grasps divided by the total number of objects. Each scene is terminated after two consecutive grasp failures or detection failures. We created 128 scenes with the mesh models provided by Breyer et al. [5]³ which are used by [6], [8] also.

Even though some existing works evaluated their performance against various *geometric properties* (such as shape), there are limited examples that evaluate against various *physical properties* such as object weight or friction coefficient. In this work, we propose to evaluate the grasp against a varying object weight, since in the light-weight region, it captures whether the hand can *reach* the object, while in the heavy-weight region, it captures whether the hand can *lift* the object. Note that the capability to lift heavier objects is equivalent to the capability to lift the same objects with less grasp force, which is critical for handling fragile objects.

Figure 8 plots the SR and CR against the object weight from 0.1 kg to 1.5 kg. In the light-weight region (less than 0.5 kg), *Ours-Precision* performed similarly with *VGN* while *VN-EdgeGraspNet* outperformed both. This is reasonable because we share the same backbone as *VGN*, and the author of *VN-EdgeGraspNet* reported that their grasp representation is more advantageous. In the heavy-weight region (more than 1 kg), however, *Ours-Precision* outperformed *VGN* and performed on par with *VN-EdgeGraspNet*. This indicates that even limited to precision grasping, our *gravity-rejection score* is beneficial in grasping heavy objects. One hypothesis is that if the hand only supports precision grasping, introducing the *gravity-rejection score* to the edge-grasp representation will provide a better score. Nevertheless, our focus is on leveraging power grasp. *Ours*, with all features including power grasp annotation, significantly outperformed the others, with 20.9 % improvement for both SR and CR in the case of 0.1 kg and 41.9 / 48.7 % improvement of SR / CR in the case

³We merged the two test mesh sets for *packed* and *pile* and removed those that didn't fit our hand.

TABLE I
SUCCESS RATIO (SR) AND CLEAR RATIO (CR) UNDER DIFFERENT ROTATION REPRESENTATION

	Rotation Matrix (e_x - e_z)	Rotation Matrix (e_y - e_z)	Quaternion
SR [%]	71.7	68.0	57.8
CR [%]	74.1	69.2	61.0

of 1.5 kg compared with *VN-EdgeGraspNet*. Its superiority in the light-weight region indicates that power grasping is robust against positioning error, and that in the heavy-weight region indicates that it's robust against gravity.

C. Comparison on the Rotation Representation

Following Qin et al. [2], we also select rotation matrix as the rotation representation due to its continuity in the $SO(3)$. However, [2] lacks a discussion on how to select the basis vectors of the rotation matrix, i.e., how we should define the TCP coordinate. A rotation matrix $R = [e_x, e_y, e_z] \in \mathbb{R}^{3 \times 3}$ is constructed by three basis vectors. The network estimates two of them \tilde{e}_x, \tilde{e}_z and reconstructs R by:

$$\begin{aligned}
 e_x &= \tilde{e}_x / |\tilde{e}_x| \\
 e_z &= e'_z / |e'_z|, e'_z = \tilde{e}_z - (e_x \cdot \tilde{e}_z)e_x \\
 e_y &= e_z \times e_x
 \end{aligned} \quad (2)$$

which means it prioritizes \tilde{e}_x to decide two dimensions of the rotation and supplementarily uses \tilde{e}_z to decide the remaining one, while doesn't explicitly estimate the e_y direction. We name this order as e_x - e_z and compare it with the opposite order e_y - e_z , in addition to a quaternion version (see Fig. 4 left for the TCP coordinate definition.) Table I summarizes the result. In addition to the large gap between the rotation matrix and quaternion, we also observe an improvement of e_x - e_z over e_y - e_z . This indicates that e_x is easier for the network to learn than e_y . In the other part of this paper, we learn e_x and e_z , and use e_x - e_z order for the inference.

D. Validation with a Physical System

In this subsection, we validate our approach with a physical system, as shown in Fig. 9. Since we only have physical access to the Robotiq hand, we trained a baseline version of our model to mimic [5] by (i) training data only contained precision grasps, (ii) we only used *grasp validness* and ignored *gravity-rejection score* for the inference, (iii) quaternion rotation representation. We selected nine kinds of objects from the YCB dataset [27], which we didn't use for training, and created 20 scenes with 51 objects in total in a simulator. In the real system, we overlaid the scene's mesh with the real-time-streamed point cloud and manually adjusted the objects' pose in the real world. Depth image was acquired from a pair of RGB cameras and a learning-based stereo inference [28]. Table II summarizes the result, showing a significant improvement in our approach over the baseline. Note that we cannot compare the absolute SR / CR with the simulation evaluation in V-B due to the sim-to-real



Fig. 9. Target objects (left) and capture (middle, right) of the validation with a physical system.

TABLE II
SUCCESS RATIO (SR) AND CLEAR RATIO (CR) IN THE REAL ROBOT
VALIDATION

	Objects	Trials	Success	SR [%]	CR [%]
Ours	51	51	38	74.5	74.5
Baseline	51	48	31	64.6	60.8

gap. Nevertheless, we can observe a consistent result that our approach outperforms the baselines in both environments.

VI. CONCLUSION

In this paper, we presented a data generation and learning framework to leverage power grasping in addition to precision grasping. We proposed to train a neural network against the continuous *gravity-rejection score*, that is the magnitude of disturbance in the gravity direction a grasp can support, rather than the grasp probability, in order to let the network prioritize power grasping while still keeping precision grasping as a secondary choice. We also proposed a data generation pipeline to efficiently create a dataset with *gravity-rejection score* annotation. We provided a qualitative visualization and analysis of the network output and showed the effect of the combination of *gravity-rejection score* head and *grasp validness* head. For the quantitative evaluation, we proposed to evaluate the performance against varying object weights. A simulation evaluation proved a significant improvement in our approach, where power grasping improves the grasp robustness in both positioning accuracy error and gravity direction force disturbance. Finally, we provided real robot validation, which showed that our approach is also effective in a physical system.

REFERENCES

- [1] J. R. Napier, "The prehensile movements of the human hand," *The Journal of bone and joint surgery. British volume*, vol. 38, no. 4, pp. 902–913, 1956.
- [2] Y. Qin, R. Chen, H. Zhu, M. Song, J. Xu, and H. Su, "S4g: Amodal single-view single-shot se (3) grasp detection in cluttered scenes," in *Conf. on Robot Learning*. PMLR, 2020, pp. 53–65.
- [3] B. Zhao, H. Zhang, X. Lan, H. Wang, Z. Tian, and N. Zheng, "Regnet: Region-based grasp network for end-to-end grasp detection in point clouds," in *Int'l. Conf. on Robotics and Automation*. IEEE, 2021, pp. 13 474–13 480.
- [4] M. Sundermeyer, A. Mousavian, R. Triebel, and D. Fox, "Contact-graspnet: Efficient 6-dof grasp generation in cluttered scenes," in *Int'l. Conf. on Robotics and Automation*. IEEE, 2021, pp. 13 438–13 444.
- [5] M. Breyer, J. J. Chung, L. Ott, R. Siegwart, and J. Nieto, "Volumetric grasping network: Real-time 6 dof grasp detection in clutter," in *Conf. on Robot Learning*. PMLR, 2021, pp. 1602–1611.

- [6] Z. Jiang, Y. Zhu, M. Svetlik, K. Fang, and Y. Zhu, "Synergies between affordance and geometry: 6-dof grasp detection via implicit representations," *arXiv preprint arXiv:2104.01542*, 2021.
- [7] C. Wang, H.-S. Fang, M. Gou, H. Fang, J. Gao, and C. Lu, "Graspness discovery in cluttered scenes for fast and accurate grasp detection," in *Int'l. Conf. on Computer Vision*. IEEE/CVF, 2021, pp. 15 964–15 973.
- [8] H. Huang, D. Wang, X. Zhu, R. Walters, and R. Platt, "Edge grasp network: A graph-based se (3)-invariant approach to grasp detection," *arXiv preprint arXiv:2211.00191*, 2022.
- [9] J. Cai, J. Cen, H. Wang, and M. Y. Wang, "Real-time collision-free grasp pose detection with geometry-aware refinement using high-resolution volume," *IEEE Robotics and Automation Letters*, vol. 7, no. 2, pp. 1888–1895, 2022.
- [10] B. Siciliano, O. Khatib, and T. Kröger, "Design of robot hands," in *handbook of robotics*. Springer, 2008, ch. 15.2, pp. 347–351.
- [11] Robotiq, "2f-85 and 2f-140 grippers," 2024. [Online]. Available: <https://robotiq.com/products/2f85-140-adaptive-robot-gripper>
- [12] J. Mahler, J. Liang, S. Niyaz, M. Laskey, R. Doan, X. Liu, J. A. Ojea, and K. Goldberg, "Dex-net 2.0: Deep learning to plan robust grasps with synthetic point clouds and analytic grasp metrics," *arXiv preprint arXiv:1703.09312*, 2017.
- [13] J. Weisz and P. K. Allen, "Pose error robust grasping from contact wrench space metrics," in *Int'l. Conf. on Robotics and Automation*. IEEE, 2012, pp. 557–562.
- [14] H.-S. Fang, C. Wang, M. Gou, and C. Lu, "Graspnet-1billion: A large-scale benchmark for general object grasping," in *Conf. on Computer Vision and Pattern Recognition*. IEEE/CVF, 2020, pp. 11 444–11 453.
- [15] H.-S. Fang, C. Wang, H. Fang, M. Gou, J. Liu, H. Yan, W. Liu, Y. Xie, and C. Lu, "Anygrasp: Robust and efficient grasp perception in spatial and temporal domains," *IEEE Transactions on Robotics*, 2023.
- [16] C. Ferrari and J. F. Canny, "Planning optimal grasps," in *Int'l. Conf. on Robotics and Automation*, vol. 3, no. 4. IEEE, 1992, p. 6.
- [17] D. Kappler, J. Bohg, and S. Schaal, "Leveraging big data for grasp planning," in *Int'l. Conf. on Robotics and Automation*. IEEE, 2015, pp. 4304–4311.
- [18] Y. Zhou and K. Hauser, "6dof grasp planning by optimizing a deep learning scoring function," in *RSS workshop on revisiting contact-turning a problem into a solution*, vol. 2, 2017, p. 6.
- [19] C. Eppner, A. Mousavian, and D. Fox, "Acronym: A large-scale grasp dataset based on simulation," in *Int'l. Conf. on Robotics and Automation*. IEEE, 2021, pp. 6222–6227.
- [20] M. Gualtieri, A. Ten Pas, K. Saenko, and R. Platt, "High precision grasp pose detection in dense clutter," in *Int'l. Conf. on Intelligent Robots and Systems*. IEEE/RSJ, 2016, pp. 598–605.
- [21] A. Mousavian, C. Eppner, and D. Fox, "6-dof graspnet: Variational grasp generation for object manipulation," in *Int'l. Conf. on Computer Vision*. IEEE/CVF, 2019, pp. 2901–2910.
- [22] H. Liang, X. Ma, S. Li, M. Görner, S. Tang, B. Fang, F. Sun, and J. Zhang, "Pointnetgpd: Detecting grasp configurations from point sets," in *Int'l. Conf. on Robotics and Automation*. IEEE, 2019, pp. 3629–3635.
- [23] D. Morrison, P. Corke, and J. Leitner, "Closing the Loop for Robotic Grasping: A Real-time, Generative Grasp Synthesis Approach," in *Robotics: Science and Systems*, 2018.
- [24] S. Haddadin, S. Parusel, L. Johannsmeier, S. Golz, S. Gabl, F. Walch, M. Sabaghian, C. Jähne, L. Hausperger, and S. Haddadin, "The franka emika robot: A reference emka platform for robotics research and education," *IEEE Robotics & Automation Magazine*, vol. 29, no. 2, pp. 46–64, 2022.
- [25] R. Tedrake and the Drake Development Team, "Drake: Model-based design and verification for robotics," 2019. [Online]. Available: <https://drake.mit.edu>
- [26] R. Elandt, E. Drumwright, M. Sherman, and A. Ruina, "A pressure field model for fast, robust approximation of net contact force and moment between nominally rigid objects," in *Int'l. Conf. on Intelligent Robots and Systems*. IEEE/RSJ, 2019, pp. 8238–8245.
- [27] B. Calli, A. Singh, A. Walsman, S. Srinivasa, P. Abbeel, and A. M. Dollar, "The ycb object and model set: Towards common benchmarks for manipulation research," in *Int'l. Conf. on Advanced Robotics*. IEEE, 2015, pp. 510–517.
- [28] K. Shankar, M. Tjersland, J. Ma, K. Stone, and M. Bajracharya, "A learned stereo depth system for robotic manipulation in homes," *IEEE Robotics and Automation Letters*, vol. 7, no. 2, pp. 2305–2312, 2022.